Monthly Notices
of the
ROYAL ASTRONOMICAL SOCIETY

MNRAS **470,** 4600–4607 (2017)
Advance Access publication 2017 June 22

doi:10.1093/mnras/stx1572

Further observational evidence for a critical ionizing luminosity in active galaxies

S. J. Curran,[1⋆] R. W. Hunstead,[2] H. M. Johnston,[2] M. T. Whiting,[3] E. M. Sadler,[2] J. R. Allison[3] and C. Bignell[4]

[1]*School of Chemical and Physical Sciences, Victoria University of Wellington, PO Box 600, Wellington 6140, New Zealand*
[2]*Sydney Institute for Astronomy, School of Physics, The University of Sydney, NSW 2006, Australia*
[3]*CSIRO Astronomy and Space Science, PO Box 76, Epping, NSW 1710, Australia*
[4]*National Radio Astronomy Observatory, PO Box 2, Rt. 28/92 Green Bank, WV 24944-0002, USA*

Accepted 2017 June 20. Received 2017 June 1; in original form 2017 April 13

ABSTRACT

We report the results of a survey for H I 21-cm absorption at redshifts of $z \gtrsim 2.6$ in a new sample of radio sources with the Green Bank and Giant Metrewave Radio Telescopes. From a total of 25 targets, we report zero detections in the 16 for which optical depth limits could be obtained. Based upon the detection rate for $z \geq 0.1$ associated absorption, we would expect approximately four detections. Of the 11 which have previously not been searched, there is sufficient source-frame optical/ultraviolet photometry to determine the ionizing photon rate for four. Adding these to the literature, the hypothesis that there is a critical rate of $Q_{\rm H\,I} \sim 10^{56}$ ionizing photons per second (a monochromatic $\lambda = 912$ Å luminosity of $L_{\rm UV} \sim 10^{23}$ W Hz^{-1}) is now significant at $\approx 7\sigma$. This reaffirms our assertion that searching $z \gtrsim 3$ active galaxies for which optical redshifts are available selects sources in which the ultraviolet luminosity is sufficient to ionize all of the neutral gas in the host galaxy.

Key words: galaxies: active – galaxies: fundamental parameters – galaxies: ISM – quasars: absorption lines – radio lines: galaxies.

1 INTRODUCTION

While absorption of the 21-cm spin-flip transition of neutral hydrogen (H I) is readily detected in near-by galaxies, it is conspicuous by its absence from the redshifted Universe. H I 21-cm absorption traces the cool component of the gas, the reservoir for star formation, which can be detected in either quiescent galaxies *intervening* the line of sight to a more distant radio source or *associated* with the host galaxy of the radio source itself. While the detection of hydrogen at radio wavelengths is not susceptible to the dust extinction effects of optical/ultraviolet band searches (Carilli et al. 1998; Curran et al. 2006, 2017), after over three decades of searching (e.g. Davis & May 1978; de Waard, Strom & Miley 1985) there are only 50 detections each of H I 21-cm at $z \gtrsim 0.1$ in either intervening or associated absorption (compiled in Curran et al. 2016b). This is despite H I being detected through Lyman-α absorption in 12 000 damped Lyman-α absorbers (DLAs) and sub-DLAs[1] (Noterdaeme et al. 2012), mainly at $z \gtrsim 1.7$, where the Lyman-α transition is redshifted into the atmospheric observing window.[2] By comparison, the detection of H I 21-cm absorption occurs overwhelmingly at redshifts of $z \lesssim 1$, or less than half the look-back time to the origin of the Universe. While much of this can be attributed to the past availability of the suitable radio bands, detection rates at $z \gtrsim 1$ are demonstrably lower than at $z \lesssim 1$ (Kanekar & Chengalur 2003; Curran et al. 2013c).

For the intervening absorbers, it has been argued that this is due to an evolution in the spin temperature, $T_{\rm s}$, of the gas, where the fraction of the cold neutral medium (CNM, where $T \sim 150$ K and $n \sim 10$ cm^{-3}) decreases with redshift (Kanekar & Chengalur 2003; Kanekar et al. 2014). However, given that the comparison of the 21-cm absorption strength with the total neutral hydrogen column density, from the Lyman-α transition, can at best yield the spin temperature/covering factor degeneracy ($T_{\rm s}/f$), Curran et al. (2005) argued that an apparent evolution in $T_{\rm s}$ could be caused by the assumption that $f = 1$ for the high redshift absorbers. Furthermore, by accounting for the effects of an expanding Universe, a standard Λ

⋆ E-mail: scurran.astro@gmail.com

[1] A DLA is defined as having a neutral hydrogen column density exceeding $N_{\rm H\,I} = 2 \times 10^{20}$ atoms cm^{-2}, with sub-DLAs having lower column densities, although exhibiting the same characteristic damping wings in the absorption profile.

[2] At lower redshifts, a high H I column density is inferred from the equivalent width of the Mg II absorption and other metal ion transitions that can be detected by ground-based telescopes (e.g. Rao, Turnshek & Nestor 2006).

cosmology means that at redshifts of $z \gtrsim 1$, the absorber is always at a similar angular diameter distance as the background continuum source, i.e. $DA_{\rm abs} \approx DA_{\rm QSO}$. In contrast, at $z \lesssim 1$, $DA_{\rm abs} < DA_{\rm QSO}$ is possible (when $z_{\rm abs} < z_{\rm QSO}$), suggesting that the mix of 'spin temperatures' at $z \lesssim 1$ and exclusively high values at $z \gtrsim 1$ (Kanekar & Chengalur 2003) is in fact the effect of geometry on the covering factor (Curran & Webb 2006; Curran 2012). By deconstructing the covering factor, via the angular diameter distances and high resolution imaging of the background sources, there is now compelling evidence that the fraction of the CNM in intervening absorbers may trace the star formation history of the Universe (Curran 2017).

For the associated absorbers, since, by definition, $z_{\rm abs} \approx z_{\rm QSO}$, the same geometric effects cannot account for the difference in the detection rates between the low- and high-redshift sources. From a survey of H I 21-cm absorption at $z \gtrsim 3$, Curran et al. (2008) suggested that their exclusively non-detections were due to the high redshifts selecting sources with high rest-frame ultraviolet luminosities ($L_{\rm UV} \gtrsim 10^{23}$ W Hz^{-1}). Since an examination of the literature showed that H I 21-cm had never been detected at these luminosities, irrespective of redshift, they suggested that the non-detection of cool neutral gas was due to the high-redshift selection yielding only sources where the UV luminosity was sufficient to excite the gas to below the detection limit. This observational result has since been confirmed several times for various heterogeneous samples (Curran et al. 2011a, 2013b,c, 2016a, 2017; Allison et al. 2012; Geréb et al. 2015; Aditya, Kanekar & Kurapati 2016; Grasha et al. 2017),[3] showing this to be an ubiquitous effect.

In order to investigate why there is an apparent critical UV luminosity and why this is $L_{\rm UV} \sim 10^{23}$ W Hz^{-1}, Curran & Whiting (2012) applied the equation of photoionzation equilibrium (Osterbrock 1989) to a gas disc with an exponential density distribution (Begeman, Broeils & Sanders 1991), and found that an ionizing photon rate of $Q_{\rm H\,I} \equiv \int_{\nu}^{\infty} (L_{\nu}/h\nu)\,{\rm d}\nu \approx 3 \times 10^{56}$ s^{-1} (a monochromatic $\lambda = 912$ Å luminosity of $L_{\rm UV} \sim 10^{23}$ W Hz^{-1}) will ionize a gas disc with the same scalelength as the Milky Way (Kalberla et al. 2007). This suggests that the observed critical luminosity is sufficient to ionize all of the neutral gas in a large spiral galaxy, thus explaining why H I 21-cm has never been detected where $L_{\rm UV} \gtrsim 10^{23}$ W Hz^{-1}. Since the vast majority of $z \gtrsim 1$ radio sources for which redshifts are available are believed to have luminosities above the critical value (see fig. 4 of Morganti et al. 2015), this would mean that even the Square Kilometre Array (SKA) will be unable to detect H I 21-cm absorption in these objects.

Given this critical luminosity above which all of the gas in the host is ionized, in order to detect the cool, star-forming gas within high-redshift radio sources, we need to dispense with the reliance upon an optical redshift, thus avoiding the selection of the most UV luminous objects. Through their wide instantaneous bandwidths, the SKA pathfinders are ideally suited to spanning a large range of redshift space in a single tuning (e.g. Allison et al. 2015; Maccagni et al. 2017).[4] However, these are generally limited to frequencies of $\gtrsim 700$ MHz, i.e. H I 21-cm at redshifts of $z \lesssim 1$, therefore requiring the SKA to find the missing cold neutral gas at high redshift. In the meantime, we can continue to search for H I 21-cm absorption, via various search strategies, with currently available instruments (e.g. Curran et al. 2016a). From newly obtained redshifts for a sample of strong flat spectrum radio sources (see Section 2.1), we can perform a large survey for associated 21-cm absorption in active galaxies over redshift ranges spanning most of the Universe's history. Here, we present the results of our high-redshift ($z \gtrsim 2.6$) survey with the Green Bank Telescope (GBT) and the Giant Metrewave Radio Telescope (GMRT).

[3] Grasha et al. (2017), which is still in submission, report 0 new detections of H I 21-cm absorption out of 89 new searches over $0.02 < z < 3.8$ (see Grasha & Darling 2011).

[4] Since the nature of the absorber is usually determined from an optical spectrum, other techniques for distinguishing intervening from associated absorption must be explored, with machine learning showing some promise (Curran et al. 2016b).

2 OBSERVATIONS AND ANALYSIS

2.1 The sample

The *Second Realization of the International Celestial Reference Frame by Very Long Baseline Interferometry* (ICRF2, Ma et al. 2009) constitutes a sample of strong flat spectrum radio sources, of which 1682 now have known redshifts (Titov & Malkin 2009; Titov et al. 2013, and references therein), yielding a tuning frequency in the search for 21-cm absorption. Being VLBI sources, all have significant compact flux, thus maximizing the chance of a high covering factor and thus optical depth (Curran et al. 2013a). The original aim of the survey was to form part of a large observing campaign to search and quantify the incidence of associated H I 21-cm absorption over all redshifts, although observing time was only granted for the high-redshift ($z \gtrsim 2.6$) proposals. As mentioned above (Section 1), we believe that such a high-redshift selection will yield only sources above the critical UV luminosity, where the detection of H I 21-cm is unlikely. However, having a preconceived suspicion of the outcome should not preclude it from being tested.

2.2 Observations and data reduction

2.2.1 GBT observations

In the ICRF2, 1456 of the sources have declinations accessible to the GBT, in addition to being at a redshift that places the 21-cm transition into a GBT band. For this, the high-redshift survey, we used the PF1 290–395 MHz receiver (H I 21-cm over $z = 2.6$–3.9). We formed our target list by prioritizing sources with flux densities estimated to be in excess of 1 Jy at the redshifted 21-cm frequency. Excluding the two that already had published searches at the time, we were left with 24 targets. The observations were performed over 2014 February 24–26 with each source observed for a total of 1.3 h in two orthogonal linear polarizations (XX and YY). The Prime Focus 1 (PF1) receiver was used, backed by the GBT spectrometer, with a bandwidth of 12.5 MHz, in order to minimize RFI while maintaining a velocity coverage of $\Delta v \approx \pm 5500$ km s^{-1}. A channel width of 11 kHz gave a spectral resolution of $\approx$10 km s^{-1}. The data were analysed, flagged for RFI and averaged using the GBTIDL software.

2.2.2 GMRT observations

In the ICRF2, 416 of the sources have declinations accessible to the GMRT, of which 54 have 21-cm shifted to within the 90-cm band (305–360 MHz, H I 21-cm over $z = 2.9$–3.7). We prioritized sources with flux densities estimated to be in excess of 0.5 Jy at the redshifted 21-cm frequency. As per the GBT observations, the flux limit was chosen in order to attain high sensitivities, while still retaining a sizable number of targets. If the radio luminosity is correlated with the UV luminosity, it is conceivable that this selection may bias against the detection of cool, neutral gas. Although there is

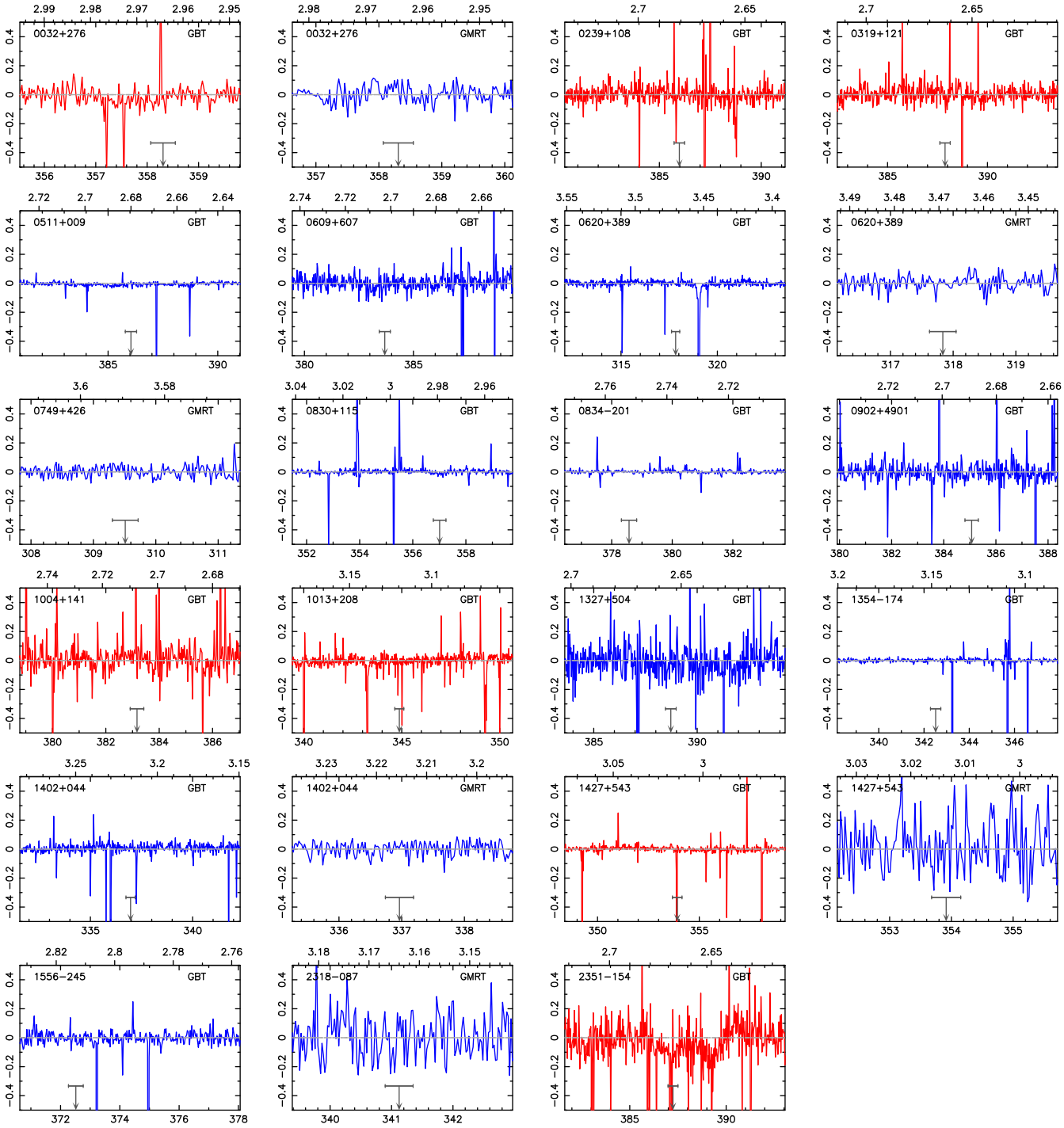

Figure 1. The reduced spectra, for which optical depth limits could be derived (Table 1), at a spectral resolution of 20 km s^{-1}. The ordinate gives the observed optical depth and the abscissa the barycentric frequency (MHz). The scale along the top of each panel shows the redshift of H I 21-cm over the frequency range and the downwards arrow shows the expected frequency of the absorption from the optical redshift, with the horizontal bar showing a span of ±200 km s^{-1} for guidance (the profile widths of the 21-cm detections range from 18 to 475 km s^{-1}, with a mean of 167 km s^{-1}). The traces in red have a significant RFI spike within this range, thus potentially masking a detection. These spectra are not included in any further analysis.

a relationship (Curran & Whiting 2010), there is no critical rest-frame 1.4-GHz luminosity (Curran et al. 2008), with the relationship probably arising from both luminosities being correlated with the redshift.

Excluding the potential targets with published searches for 21-cm absorption at the time left 16 targets. The observations were taken with the full 30 antenna array over 2013 November 9–13 and 2014 March 28–29, with each source observed for a total of 2 hr in two orthogonal circular polarizations (LL and RR). For bandpass calibration 3C 48, 3C 147 and 3C 298 were used, with the phases being self-calibrated apart from 1427+543, 1427+543, 0521–262 and 2318–087, which used a strong near-by unresolved source. For

Table 1. The observational results by IAU name (B1950 designation, see Table 2 for the full names as resolved by the NASA/IPAC Extragalactic Database). z is the optical redshift of the source, ΔS the rms noise reached per 20 km s^{-1} channel, $S_{\rm meas}$ is the measured flux density, $\tau_{3\sigma}$ the derived optical depth limit, where $\tau_{3\sigma} = -\ln(1 - 3\Delta S/S_{\rm meas})$ is quoted for these non-detections. These give the quoted column densities, where $T_{\rm s}$ is the spin temperature and f the covering factor; a blank field indicates that the observations were dominated by RFI or the presence of an RFI/instrumental spike close to the expected absorption redshift. The final two columns give the frequency and redshift range over which the limit applies (neglecting the spikes).

Source	z	Tel.	ΔS (mJy)	$S_{\rm meas}$ (Jy)	$\tau_{3\sigma}$	$N_{\rm H\,I}$ (cm^{-2})	ν-range (MHz)	z-range
0032+276	2.9642	GBT	57	1.250	<0.14	–	354.23–359.83	2.9474–3.0099
–	–	GMRT	38	0.676	<0.17	$<6.1 \times 10^{18}\,(T_{\rm s}/f)$	356.50–360.33	2.9420 –2.9843
0239+108[a]	2.6800	GBT	48	1.032	<0.14	–	380.48–391.06	2.6322–2.7332
0319+121[b]	2.6620	GBT	61	1.510	<0.12	–	382.51–393.83	2.6067–2.7134
0511+009	2.6794	GBT	64	5.208	<0.04	$<1.3 \times 10^{18}\,(T_{\rm s}/f)$	380.71–390.73	2.6352–2.7309
0521−262	3.109	GMRT	–	–	–	– -	RFI DOMINANT	
0609+607	2.7020	GBT	54	1.364	<0.12	$<4.4 \times 10^{18}\,(T_{\rm s}/f)$	378.74–389.48	2.6469–2.7503
0620+389[c]	3.4690	GBT	44	2.926	<0.05	$<1.6 \times 10^{18}\,(T_{\rm s}/f)$	312.11–323.60	3.3894–3.5509
–	–	GMRT	11	0.226	<0.14	$<5.0 \times 10^{18}\,(T_{\rm s}/f)$	315.92–319.75	3.4422–3.4961
0749+426[d]	3.5892	GMRT	19	0.771	<0.07	$<2.7 \times 10^{18}\,(T_{\rm s}/f)$	307.60–311.43	3.5609–3.6177
0800+618[e]	3.0330	GMRT	–	–	–	–	RFI DOMINANT	
0830+115	2.9786	GBT	35	3.906	<0.04	$<1.3 \times 10^{18}\,(T_{\rm s}/f)$	351.37–359.90	2.9467–3.0425
0834–201	2.7520	GBT	78	4.223	<0.06	$<2.0 \times 10^{18}\,(T_{\rm s}/f)$	375.10–384.38	2.6953–2.7868
0902+490[f]	2.6887	GBT	60	0.916	<0.20	$<7.2 \times 10^{18}\,(T_{\rm s}/f)$	379.26–390.94	2.6334–2.7452
0913+003	3.074	GMRT	–	–	–	–	RFI DOMINANT	
1004+141[g]	2.7070	GBT	110	0.614	<0.77[h]	–	378.66–386.95	2.6708–2.7511
1013+208	3.1186	GBT	42	1.094	<0.12	–	340.34–350.54	3.0521–3.1735
1327+504	2.6540	GBT	69	0.682	<0.30	$<1.1 \times 10^{19}\,(T_{\rm s}/f)$	383.69–394.47	2.6008–2.7020
1354−174	3.1470	GBT	41	3.912	<0.03	$<1.1 \times 10^{18}\,(T_{\rm s}/f)$	337.49–347.84	3.0836–3.2088
1402+044	3.2153	GBT	53	1.429	<0.11	$<4.1 \times 10^{18}\,(T_{\rm s}/f)$	331.44–342.91	3.1422–3.2856
–	–	GMRT	17	0.351	<0.15	$<5.3 \times 10^{18}\,(T_{\rm s}/f)$	335.04–338.88	3.1915–3.2395
1427+543	3.0134	GBT	47	2.606	<0.05	–	348.32–359.74	2.9484–3.0779
–	–	GMRT	68	0.429	<0.65[h]	$<2.4 \times 10^{19}\,(T_{\rm s}/f)$	352.00–355.83	2.9918–3.0352
1446−111	2.6326	GBT	75	0.038	–	–	385.43–396.71	2.5805–2.6852
1556−245	2.8130	GBT	65	1.754	<0.11	$<4.1 \times 10^{18}\,(T_{\rm s}/f)$	369.89–378.24	2.7553–2.8401
1614+051	3.2150	GMRT	11	0.024	–	–	335.07–338.90	3.1912–3.2391
1745+624	3.8890	GBT	67	0.045	–	–	285.20–296.26	3.7945–3.9805
2318−087	3.1639	GMRT	74	0.505	<0.56[h]	$<2.0 \times 10^{19}\,(T_{\rm s}/f)$	339.21–343.04	3.1406–3.1874
2351−154	2.6680	GBT	81	0.794	<0.37[h]	–	381.41–393.10	2.6133–2.7241

Notes. [a]Observed by Grasha et al. (2017) but ruined by RFI, [b]$N_{\rm H\,I} < 6.3 \times 10^{17}\,(T_{\rm s}/f)$ per 30 km s^{-1} by Grasha et al. (2017), [c]$N_{\rm H\,I} < 3.6 \times 10^{17}\,(T_{\rm s}/f)$ per 30 km s^{-1} by Aditya et al. (2016), [d]$N_{\rm H\,I} < 1.4 \times 10^{18}\,(T_{\rm s}/f)$ per 30 km s^{-1} by Aditya et al. (2016), [e]$N_{\rm H\,I} < 2.1 \times 10^{18}\,(T_{\rm s}/f)$ per 26 km s^{-1} by Aditya et al. (2016), [f]$N_{\rm H\,I} < 1.5 \times 10^{18}\,(T_{\rm s}/f)$ per 30 km s^{-1} by Grasha et al. (2017), 1004+141, [g]$N_{\rm H\,I} < 1.5 \times 10^{18}\,(T_{\rm s}/f)$ per 30 km s^{-1} by Grasha et al. (2017). [h]Since $\tau \gtrsim 0.3$, the optical depth limit is derived assuming $f = 1$ (see Curran et al. 2017).

the backend we used the FX correlator over a bandwidth of 4 MHz, which over 512 channels gave a spectral resolution of ≈7 km s^{-1}. The data were calibrated and flagged using the MIRIAD interferometry reduction package. After averaging the two polarizations, a spectrum was extracted from the cube. None of the sources was resolved by the synthesized beam, which ranged from 10.7 × 9.4 arcsec^2 to 30.2 × 11.1 arcsec^2.

3 RESULTS

3.1 Observational results

Of the 29 spectra, three were completely dominated by RFI and a further three had close to zero flux. In Fig. 1, we show the remaining 23 spectra, from 19 different targets. Of these, seven have RFI/instrumental spikes close to the expected frequency of the putative absorption, which may conceal any possible detection (Table 1).[5] This leaves 16 good spectra of 14 different targets, 11 of which have not been previously searched.

In the optically thin regime (where $\tau \lesssim 0.3$), the total neutral hydrogen column density is related to the velocity integrated optical depth of the H I 21-cm absorption via

$$N_{\rm H\,I} \approx 1.823 \times 10^{18} \frac{T_{\rm s}}{f} \int \tau \, {\rm d}v,$$

where $T_{\rm s}$ is the spin temperature of the gas, which is a measure of the excitation from the lower hyperfine level (Purcell & Field 1956; Field 1959) and $\int \tau {\rm d}v$ is the observed velocity integrated optical depth of the absorption. In order to compare our limits with previous surveys, all spectra are re-sampled to the same spectral resolution (20 km s^{-1}, as in Fig. 1), which is used as the FWHM to obtain the integrated optical depth limit, thus giving the $N_{\rm H\,I} f/T_{\rm spin}$ limit per channel (see Curran 2012).

Of the 11 new sources searched, for which a limit could be obtained, there were no detections of H I 21-cm absorption. Although the limits are not as sensitive as many of the other searches,

[5] All of the spikes arise in spectra taken with the GBT, since the single dish limits the options to mitigate the RFI. Another consequence is that the large beam at these frequencies (HPBW ≈ 40 arcmin) means that the off-measurement is very likely to contain another radio source. This will affect the flux calibration, leading to the differences from the GMRT values for the same source (which has HPBW $\lesssim$ 0.5 arcmin and no off-measurement) although the optical depths are expected to be unaffected (Ries 2012).

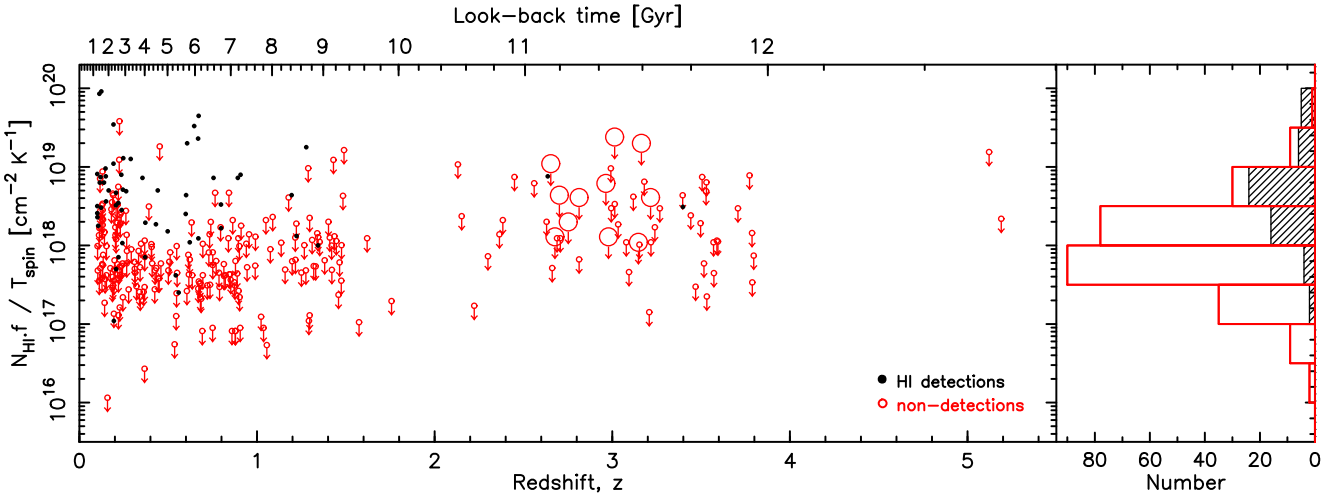

Figure 2. The line strength $[1.823 \times 10^{18}\,(T_s/f)\int \tau\,\mathrm{d}v]$ versus redshift for the $z \geq 0.1$ associated H I 21-cm absorption searches. The filled circles/histograms represent the detections and the unfilled circles/histograms represent the 3σ upper limits to the non-detections, with the large circles designating our new targets.

particularly those at low redshift (Fig. 2),[6] there are 42 detections and 116 previous non-detections over the range of sensitivities searched $[N_{\rm H\,I} = (0.1{-}2.4) \times 10^{19}\,(T_s/f)\ \mathrm{cm}^{-2}]$. This gives a detection rate of 27 per cent over all redshifts within these sensitivity limits, which is close to the overall detection rate (30.5 per cent, Section 3.2) and comparable to the 25 per cent found by Gupta et al. (2006). Note that the highest detection rate, of 40 per cent, was obtained by Vermeulen et al. (2003) in a survey of $z \lesssim 1$ compact radio sources,[7] where we may expect a maximum of ≈50 per cent, due to the alignment between the gaseous disc and continuum source along our sight-line (see Curran & Whiting 2010). From binomial statistics, we therefore expect 3.8 ± 1.6 new detections for the 14 different targets with good spectra.

3.2 Ionizing photon rates

Following our usual procedure (e.g. Curran et al. 2013b), for each target we obtained the photometry from NASA/IPAC Extragalactic Database (NED), the Wide-Field Infrared Survey Explorer (WISE, Wright et al. 2010), Two Micron All Sky Survey (2MASS, Skrutskie et al. 2006) and the Galaxy Evolution Explorer (*GALEX* data release GR6/7)[8] data bases. Each flux, S_ν, was corrected for Galactic extinction (Schlegel, Finkbeiner & Davis 1998), before being converted to a specific luminosity at the source-frame frequency, via $L_\nu = 4\pi\,D_{\rm L}^2\,S_\nu/(z+1)$, where $D_{\rm L}$ is the luminosity distance to the source, given by

$$D_{\rm L} = D(z+1),\ \text{where}\ D = \frac{c}{H_0}\int_0^z \frac{\mathrm{d}z}{H_z/H_0}$$

is the line-of-sight comoving distance (e.g. Peacock 1999), in which c is the speed of light, H_0 the Hubble constant, H_z the Hubble parameter at redshift z and

$$\frac{H_z}{H_0} = \sqrt{\Omega_{\rm m}\,(z+1)^3 + (1-\Omega_{\rm m}-\Omega_\Lambda)\,(z+1)^2 + \Omega_\Lambda},$$

where we use a standard Λ cosmology, with $H_0 = 71\ \mathrm{km\,s^{-1}\,Mpc^{-1}}$, $\Omega_{\rm m} = 0.27$ and $\Omega_\Lambda = 0.73$. We then fit a power law to the

Table 2. The ionizing photon rates (photons s^{-1}) of the targets for which a limit to the absorption strength could be obtained.

NED name	IAU	z	$\log_{10} Q_{\rm H\,I}$
B2 0032+27	0032+276	2.9642	–
PKS 0239+108	0239+108	2.680	–
PKS 0319+12	0319+121	2.662	–
PMN J0513+0100	0511+009	2.6770	–
PKS 0521−262[a]	0521−262	3.109	–
BZQ J0614+6046	0609+607	2.702	–
B2 0620+38	0620+389	3.469	–
B3 0749+426	0749+426	3.5892	57.71 ± 0.78
WISE J080518.15+614424.0[a]	0800+618	3.033	–
[HB89] 0830+115	0830+115	2.9786	–
[HB89] 0834−201	0834−201	2.752	57.52 ± 0.12
SDSS J090527.46+485049.9[a]	0902+490	2.6887	57.99 ± 0.20
SDSS J091551.69+000713.2[a]	0913+003	3.074	–
[HB89] 1004+141	1004+141	2.707	–
PKS 1014+208	1013+208	3.1186	–
SDSS J132905.80+500926.5	1327+504	2.654	–
PKS 1354−17	1354−174	3.147	–
[HB89] 1402+044	1402+044	3.2153	57.04 ± 0.47
SDSS J142921.87+540611.1	1427+543	3.0134	56.69 ± 0.51
PKS B1446−111[a]	1446−111	2.6326	–
[HB89] 1556−245	1556−245	2.813	57.77 ± 0.78
[HB89] 1614+051[a]	1614+051	3.2150	–
4C +62.29[a]	1745+624	3.889	58.51 ± 0.07
PKS 2318−087	2318−087	3.1639	–
[HB89] 2351−154	2351−154	2.668	56.94 ± 0.90

Note. [a]Shown for completeness as no sensitivity limit could be derived.

[6] For example, at $z > 2$ the most sensitive limit is $N_{\rm H\,I} = 10^{17}\,(T_s/f)\ \mathrm{cm}^{-2}$, and at $z \leq 2$ there are seven searches below this limit.

[7] Not only do compact sources tend to have lower ultraviolet luminosities (Curran & Whiting 2010; Allison et al. 2012), but there is an anticorrelation between the optical depth of the 21-cm absorption and the extent of the radio source (Curran et al. 2013a).

[8] http://galex.stsci.edu/GR6/#mission

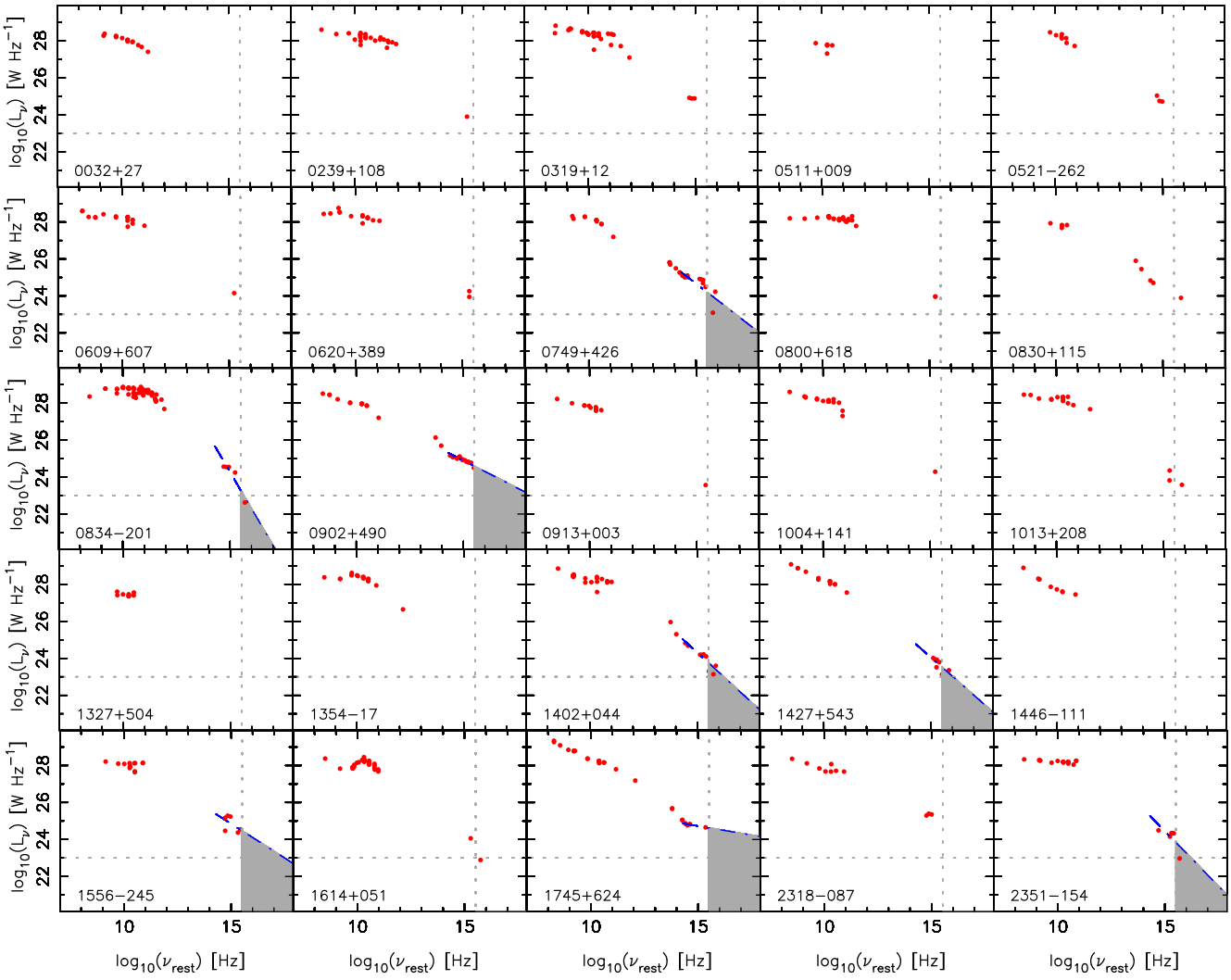

Figure 3. The rest-frame photometry for each of the 25 targets. The dashed line shows the power-law fit to the optical/UV data, the vertical dotted line signifies a rest-frame frequency of 3.29×10^{15} Hz ($\lambda = 912$ Å) and the horizontal line the critical $\lambda = 912$ Å luminosity of $L_{\rm UV} \sim 10^{23}$ W Hz^{-1}, with the shading showing the region over which the ionizing photon rate is derived (Table 2).

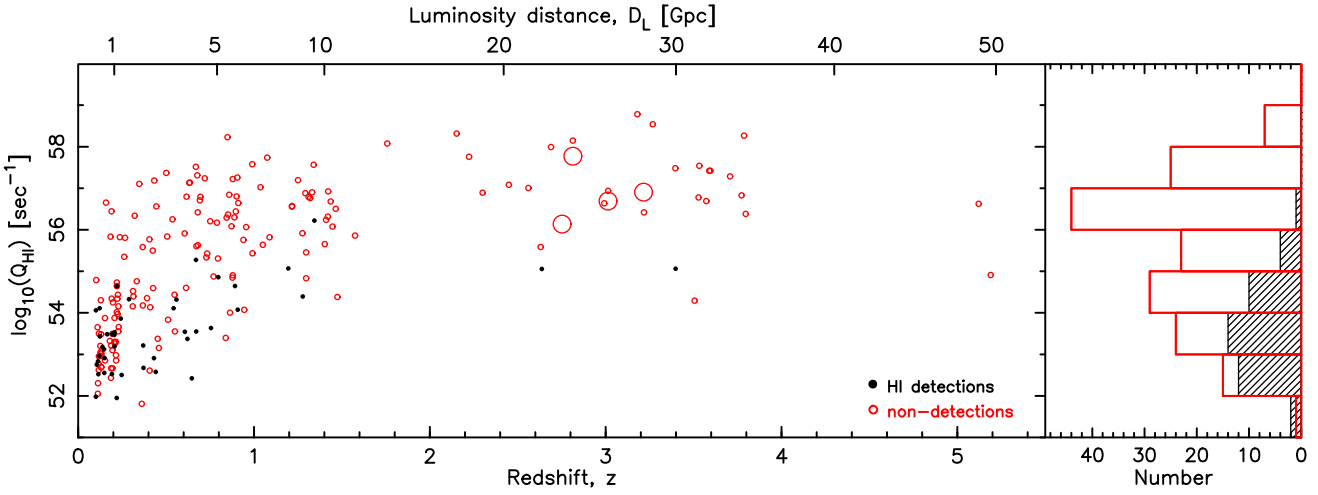

Figure 4. The ionizing ($\lambda \leq 912$ Å) photon rate versus redshift for the $z \geq 0.1$ H I 21-cm absorption searches. The symbols and histogram are as per Fig. 2, where we see that the two $z > 2$ detections are below the critical ionizing photon rate (4C +05.19 at $z = 2.64$, Moore et al. 1999 and B2 0902+34 at $z = 3.40$, Uson et al. 1991). Note that 0749+426 at $z = 3.5892$–$\log_{10} Q_{\rm H\,I} = 57.71$ is not flagged as one of our targets since this was observed to a deeper limit by Aditya et al. (2016), Table 1.

UV rest-frame data, allowing the ionizing photon rate, $Q_{\rm H\,I} \equiv \int_{\nu}^{\infty} (L_{\nu}/h\nu)\,{\rm d}\nu$, to be derived from

$$\int_{\nu}^{\infty} \frac{L_{\nu}}{h\nu}\,{\rm d}\nu, \text{ where } \log_{10} L_{\nu} = \alpha \log_{10} \nu + \mathcal{C} \Rightarrow L_{\nu} = 10^{\mathcal{C}} \nu^{\alpha},$$

α is the spectral index and $\mathcal{C}$ the intercept, which gives

$$\frac{10^{\mathcal{C}}}{h} \int_{\nu}^{\infty} \nu^{\alpha-1}\,{\rm d}\nu = \frac{10^{\mathcal{C}}}{\alpha h} \left[\nu^{\alpha}\right]_{\nu}^{\infty} = \frac{-10^{\mathcal{C}}}{\alpha h} \nu^{\alpha}, \text{ where } \alpha < 0$$

for the ionizing photon rate.

Although there was only sufficient photometry for four of the targets which also had good spectra (Fig. 3), we can add these to the previous searches (Fig. 4).[9] Of the 311 $z \geq 0.1$ sources for which limits can be obtained, 211 have sufficient photometry to determine the ionizing photon rate. Of these, there are 43 detections and 98 non-detections with ionizing photon rates up to the highest value where 21-cm absorption has been detected ($Q_{\rm H\,I} \leq 1.7 \times 10^{56}$ s^{-1}, Kanekar et al. 2009). Applying this 30.5 per cent detection rate to the $Q_{\rm H\,I} > 1.7 \times 10^{56}$ s^{-1} sources gives a binomial probability of 8.72×10^{-12} of obtaining 0 detections and 70 non-detections, which is significant at 6.83σ, assuming Gaussian statistics. This strengthens the case for a critical UV luminosity hindering the detection of H I 21-cm absorption at high redshift.

4 SUMMARY

We have undertaken a survey for associated H I 21-cm absorption at redshifts of $z = 2.6$–3.9 in 25 radio sources with the GBT and GMRT, from which we obtain zero detections. Of the 14 for which limits could be obtained, 11 are new, with 10 of these reaching optical depths of $\tau_{3\sigma} \leq 0.3$. All of the targets were selected from the sources in the *Second Realization of the International Celestial Reference Frame by Very Long Baseline Interferometry*, for which 1682 have measured redshifts spanning up to $z = 6.2$. Our intent was to undertake a large survey over all of this redshift space in order to quantify the incidence of associated H I 21-cm absorption over the history of the Universe. However, observing time was only awarded for the highest redshift sample, where we do not expect absorption due to all of the neutral gas being ionized in the $z \gtrsim 1$ sources that have a reliable optical redshift (Curran & Whiting 2012).

Nevertheless, the ICRF2 provides a large new sample of strong flat-spectrum radio sources within which to search for 21-cm absorption, and the expectation of a null result should not prevent us from testing it. Given the general ≈30 per cent detection rate at the sensitivities obtained, we expect approximately four new detections, although obtaining zero detections is within $\approx 2\sigma$ of this. In the context of all the previous searches, there still remain only two detections in this redshift range (Uson et al. 1991; Moore et al. 1999), both of which are below the ionizing photon rate of $Q_{\rm H\,I} \sim 10^{56}$ s^{-1} (a monochromatic $\lambda = 912$ Å luminosity of $L_{\rm UV} \sim 10^{23}$ W Hz^{-1}). The addition of the five new sources for which there is sufficient photometry[10] gives a binomial probability of 8.72×10^{-12} of the observed distribution occurring by chance. This is significant at 6.83σ, which supports the hypothesis that $Q_{\rm H\,I} \sim 10^{56}$ s^{-1} is sufficient to ionize all of the neutral gas in a large spiral galaxy (Curran & Whiting 2012). This appears to be an ubiquitous effect, independent of source selection and applicable over all redshifts, with the selection of sources with $Q_{\rm H\,I} \lesssim 10^{56}$ s^{-1} being required to detect neutral hydrogen. This ionizing photon rate corresponds to blue magnitudes of $B \gtrsim 22$ at $z \gtrsim 3$, for which there are currently no radio sources with a measured optical redshift known (Curran et al. 2013c; Morganti et al. 2015).

We therefore reiterate that the detection of neutral gas within the hosts of high-redshift active galaxies requires us to dispense with the usual reliance upon an optical redshift to which to define the search frequency. The way forward is through wide-band observations of radio sources of unknown redshift with the Square Kilometre Array.

ACKNOWLEDGEMENTS

We wish to thank the anonymous referee for their helpful comments, as well as Katie Grasha and Jeremy Darling for a draft manuscript of their forthcoming paper. We also thank the staff of the GMRT who have made these observations possible. GMRT is run by the National Centre for Radio Astrophysics of the Tata Institute of Fundamental Research. The National Radio Astronomy Observatory is a facility of the National Science Foundation operated under cooperative agreement by Associated Universities, Inc. This research has made use of the NASA/IPAC Extragalactic Database (NED), which is operated by the Jet Propulsion Laboratory, California Institute of Technology, under contract with the National Aeronautics and Space Administration. This research has also made use of NASA's Astrophysics Data System Bibliographic Services.

REFERENCES

Aditya J. N. H. S., Kanekar N., Kurapati S., 2016, MNRAS, 455, 4000
Aditya J. N. H. S., Kanekar K., Prochaska J. X., Day B., Lynam P., Cruz J., 2017, MNRAS, 465, 5011
Allison J. R. et al., 2012, MNRAS, 423, 2601
Allison J. R. et al., 2015, MNRAS, 453, 1249
Begeman K. G., Broeils A. H., Sanders R. H., 1991, MNRAS, 249, 523
Carilli C. L., Perlman E. S., Stocke J. T., 1992, ApJ, 400, L13
Carilli C. L., Menten K. M., Reid M. J., Rupen M. P., Yun M. S., 1998, ApJ, 494, 175
Carilli C. L., Wang R., van Hoven M. B., Dwarakanath K., Chengalur J. N., Wyithe S., 2007, AJ, 133, 2841
Chandola Y., Sirothia S. K., Saikia D. J., 2011, MNRAS, 418, 1787
Chandola Y., Gupta N., Saikia D. J., 2013, MNRAS, 429, 2380
Curran S. J., 2012, ApJ, 748, L18
Curran S. J., 2017, MNRAS, preprint (arXiv:1704.04294)
Curran S. J., Webb J. K., 2006, MNRAS, 371, 356
Curran S. J., Whiting M. T., 2010, ApJ, 712, 303
Curran S. J., Whiting M. T., 2012, ApJ, 759, 117
Curran S. J., Murphy M. T., Pihlström Y. M., Webb J. K., Purcell C. R., 2005, MNRAS, 356, 1509

[9] Compiled from de Waard et al. (1985), Mirabel (1989), van Gorkom et al. (1989), Uson, Bagri & Cornwell (1991), Carilli, Perlman & Stocke (1992), Carilli et al. (1998), Carilli et al. (2007), Moore, Carilli & Menten (1999), Peck, Taylor & Conway (1999), Peck et al. (2000), Röttgering et al. (1999), Morganti et al. (2001), Ishwara-Chandra, Dwarakanath & Anantharamaiah (2003), Vermeulen et al. (2003), Curran et al. (2006), Curran et al. (2008), Curran et al. (2011a), Curran et al. (2011b), Curran et al. (2013b), Curran et al. (2013c), Curran et al. (2016a), Curran et al. (2017), Gupta et al. (2006), Orienti, Morganti & Dallacasa (2006), Kanekar et al. (2009), Emonts et al. (2010), Salter et al. (2010), Chandola, Sirothia & Saikia (2011), Chandola, Gupta & Saikia (2013), Allison et al. (2012), Allison et al. (2015), Yan et al. (2012), Yan et al. (2016), Geréb et al. (2015), Srianand et al. (2015), Aditya et al. (2016), Aditya et al. (2017) and Grasha et al. (2017).

[10] The four new plus one searched in common with Aditya et al. (2016).

Curran S. J., Whiting M. T., Murphy M. T., Webb J. K., Longmore S. N., Pihlström Y. M., Athreya R., Blake C., 2006, MNRAS, 371, 431
Curran S. J., Whiting M. T., Wiklind T., Webb J. K., Murphy M. T., Purcell C. R., 2008, MNRAS, 391, 765
Curran S. J. et al., 2011a, MNRAS, 413, 1165
Curran S. J., Whiting M. T., Webb J. K., Athreya R., 2011b, MNRAS, 414, L26
Curran S. J., Allison J. R., Glowacki M., Whiting M. T., Sadler E. M., 2013a, MNRAS, 431, 3408
Curran S. J., Whiting M. T., Sadler E. M., Bignell C., 2013b, MNRAS, 428, 2053
Curran S. J., Whiting M. T., Tanna A., Sadler E. M., Pracy M. B., Athreya R., 2013c, MNRAS, 429, 3402
Curran S. J., Allison J. R., Whiting M. T., Sadler E. M., Combes F., Pracy M. B., Bignell C., Athreya R., 2016a, MNRAS, 457, 3666
Curran S. J., Duchesne S. W., Divoli A., Allison J. R., 2016b, MNRAS, 462, 4197
Curran S. J., Whiting M. T., Allison J. R., Tanna A., Sadler E. M., Athreya R., 2017, MNRAS, 467, 4514
Davis M. M., May L. S., 1978, ApJ, 219, 1
de Waard G. J., Strom R. G., Miley G. K., 1985, A&A, 145, 479
Emonts B. H. C. et al., 2010, MNRAS, 406, 987
Field G. B., 1959, ApJ, 129, 536
Geréb K., Maccagni F. M., Morganti R., Oosterloo T. A., 2015, A&A, 575, 44
Grasha K., Darling J., 2011, Am. Astron. Soc. Meeting Abstracts, 43, 345.02
Grasha K., Darling J. K., Bolatto A. D. Leroy A., Stocke J., 2017, ApJ, submitted
Gupta N., Salter C. J., Saikia D. J., Ghosh T., Jeyakumar S., 2006, MNRAS, 373, 972
Ishwara-Chandra C. H., Dwarakanath K. S., Anantharamaiah K. R., 2003, JA&A, 24, 37
Kalberla P. M. W., Dedes L., Kerp J., Haud U., 2007, A&A, 469, 511
Kanekar N., Chengalur J. N., 2003, A&A, 399, 857
Kanekar N., Prochaska J. X., Ellison S. L., Chengalur J. N., 2009, MNRAS, 396, 385
Kanekar N. et al., 2014, MNRAS, 438, 2131
Ma C. et al., 2009, IERS Tech. Notes, 35, 1
Maccagni F. M., Morganti R., Oosterloo T. A., Geréb K., Maddox N., 2017, A&A, preprint (arXiv:1705.00492)
Mirabel I. F., 1989, ApJ, 340, L13
Moore C. B., Carilli C. L., Menten K. M., 1999, ApJ, 510, L87
Morganti R., Oosterloo T. A., Tadhunter C. N., van Moorsel G., Killeen N., Wills K. A., 2001, MNRAS, 323, 331
Morganti R., Sadler E. M., Curran S., 2015, Proc. Sci., Cool Outflows and HI absorbers with SKA. SISSA, Trieste, PoS(AASKA14)134
Noterdaeme P. et al., 2012, A&A, 547, L1
Orienti M., Morganti R., Dallacasa D., 2006, A&A, 457, 531
Osterbrock D. E., 1989, Astrophysics of Gaseous Nebulae and Active Galactic Nuclei. University Science Books, Mill Valley, CA
Peacock J. A., 1999, Cosmological Physics. Cambridge Univ. Press, Cambridge
Peck A. B., Taylor G. B., Conway J. E., 1999, ApJ, 521, 103
Peck A. B., Taylor G. B., Fassnacht C. D., Readhead A. C. S., Vermeulen R. C., 2000, ApJ, 534, 104
Purcell E. M., Field G. B., 1956, ApJ, 124, 542
Rao S., Turnshek D., Nestor D. B., 2006, ApJ, 636, 610
Ries P. A., 2012, PhD thesis, Univ. Virginia
Röttgering H., de Bruyn G., Pentericci L., Miley G., 1999, in Röttgering H. J. A., Best P. N., Lehnert M. D., eds, Proc. Colloq. 1999, The Most Distant Radio Galaxies. Royal Netherlands Academy of Arts and Sciences, p. 113
Salter C. J., Saikia D. J., Minchin R., Ghosh T., Chandola Y., 2010, ApJ, 715, L117
Schlegel D. J., Finkbeiner D. P., Davis M., 1998, ApJ, 500, 525
Skrutskie M. F. et al., 2006, AJ, 131, 1163
Srianand R., Gupta N., Momjian E., Vivek M., 2015, MNRAS, 451, 917
Titov O., Malkin Z., 2009, A&A, 506, 1477
Titov O., Stanford L. M., Johnston H. M., Pursimo T., Hunstead R. W., Jauncey D. L., Maslennikov K., Boldycheva A., 2013, AJ, 146, 10
Uson J. M., Bagri D. S., Cornwell T. J., 1991, Phys. Rev. Lett., 67, 3328
van Gorkom J. H., Knapp G. R., Ekers R. D., Ekers D. D., Laing R. A., Polk K. S., 1989, AJ, 97, 708
Vermeulen R. C. et al., 2003, A&A, 404, 861
Wright E. L. et al., 2010, AJ, 140, 1868
Yan T., Stocke J. T., Darling J., Hearty F., 2012, AJ, 144, 124
Yan T., Stocke J. T., Darling J., Momjian E., Sharma S., Kanekar N., 2016, AJ, 151, 74

This paper has been typeset from a TEX/LATEX file prepared by the author.